Journal of Corrosion and Materials
www.corromat.com

J. Corros. Mater. (2026) 5(1), 84–97.

Operational Windows for TADF Gain Media in Organic Solid-State Lasers: An Exciton-Evacuation Framework

Miroslav Grmela[1,*]

Department of Chemical Engineering, Polytechnique, Montréal, Québec H3T 1J4, Canada

*Corresponding author: miroslav.grmela@polymtl.ca

(Received: 18 February 2026. Received in revised form: 30 April 2026. Accepted: 17 May 2026. Published online: 30 June 2026.)

Abstract

TADF solid-state lasers demand gain media that achieve stimulated emission without generating steady-state triplet excitons. Delayed fluorescent materials that exhibit reverse intersystem crossing are ideal since they convert triplet excitons into emissive singlets but neither a small energy gap nor low optical threshold are necessary criteria for laser potential. The important issue considered in this work is the question of whether TADF gain records can be divided into practical operational windows when considering threshold, photoluminescence quantum yield, delayed-emission lifetime, prompt-emission lifetime, effective triplet-harvesting energy gap, gain-wavelength and condensed-phase structure all within one record. Sixteen emitter state records have been included in this data set, comprising molecules 1a, 1b, 2a, 2b, 3, 4a-4d, 5, 6, 7, and 8 dispersed in mCBP film, polymer microspheres, mCBP microplate, mCBP microrings and neat microcrystals. Optical utility for TADF laser operation is assessed by an exciton evacuation score which favors high radiative yield and gain accessibility but discourages long delayed-fluorescence decay times, long prompt lifetime and large triplet-harvesting energy gap. Film record 2a in mCBP film is the top overall performer with $\Phi_{PL} = 0.93$, $\tau_d = 0.8$ μs, and $P_{th} = 3.3$ μJ cm^{-2}. Green resonator record 4b in neat microcrystals is the top performing resonator since it offers $\Phi_{PL} = 0.80$, $\tau_d = 2.0$ μs, $\Delta E_{eff} = 0.02$ eV and $P_{th} = 5.0$ μJ cm^{-2}. Compound 4c yields the red microcrystal route with $P_{th} = 3.0$ μJ cm^{-2}, whereas compound 7 in mCBP microplates establishes the near-infrared lasing window at 740 nm with $P_{th} = 3.6$ μJ cm^{-2}. TADF lasers whose threshold is high even when the radiative yield, exciton removal, and morphology are all good are thus more convincing than those whose threshold is low even when taken on its own.

Keywords: thermally activated delayed fluorescence; organic lasers; exciton kinetics; amplified spontaneous emission; microcrystals; triplet harvesting; optical gain.

1. Introduction

The concept of organic lasers emerged with the demonstration of coherent optical radiation in the first laser [1]. Subsequently, dye lasers demonstrated the potential of broadly tunable organic gain media with high absorption [2]. Tunable laser emission in turn confirmed the spectral tunability of organic dyes [3]. The modern field of organic solid-state lasers originated from these milestones. Conjugated polymers showed significant optical gain under specific excitation conditions [4]. The early works on polymer lasers studied the connection between electroluminescent materials and laser generation [5]. Vapor-deposition of small molecules led to lasing in organic thin films [6]. The optical gain in conjugated-polymer-based structures was characterized in detail [7]. Moreover, the connection between molecular structure, stimulated emission, and resonators in these systems was elucidated [8]. The modern organic semiconductor laser field was described in terms of the interplay between materials, waveguides, microcavities, and distributed-feedback resonators [9]. Later reviews summarized the progress in organic solid-state laser materials [10]. The geometry and fabrication of organic-laser devices were also considered as important design criteria [11]. The materials-focused study once again emphasized the need to consider both molecular structure and condensed phase [12]. Recent threshold reduction methods confirmed that control over resonator and material losses is crucial in achieving a low threshold [13]. All these results showed that organic semiconductors can provide optical gain and lasing, but also that an organic laser is never just a molecule. The gain response depends on the radiative transition, the host, the molecular packing, the resonator, the pump geometry, and the loss mechanisms that occur when a dense exciton population is generated.

The persistent problem is that the threshold regime of an organic gain medium is also a dangerous photophysical regime. Analysis of electrically pumped organic-laser operation revealed triplet and charge losses as key obstacles [14]. Triplet absorption and triplet-singlet annihilation can directly influence the operation of organic lasers [15]. Irreversible photophysical changes are also linked to degradation phenomena observed in small molecule-based devices [16]. Further analysis of the broad spectrum of degradation phenomena in these materials has been done [17]. Studies of the operation conditions have revealed chemical products that form in organic devices during their degradation [18]. These effects are far from being marginal. They define the possibility to obtain a usable gain medium from a low-threshold demonstration. The problem

becomes even more difficult in case of electrically relevant structures as statistical charge recombination inevitably generates triplets [19]. The room-temperature triplet spectroscopy demonstrates the importance of these states even under practical conditions [20]. Indirect pumping schemes, including the recently demonstrated integrated OLED-pumped organic laser, reveal that further progress in organic lasers should take into account avoidance or separation of charge- and triplet-induced losses [21].

The thermally activated delayed fluorescent emitters present a unique opportunity here. The initial studies of TADF established efficient up-conversion of triplet excitons to emissive singlets [22]. Efficient reverse intersystem crossing became a basis for the practical conversion of triplets to singlets [23]. Highly efficient delayed-fluorescence OLEDs confirmed the technological significance of this process [24]. TADF materials thus became an important tool to improve organic optoelectronics [25]. Purely organic design provided access to the enhanced exciton harvesting beyond the spin-statistical limit of prompt fluorescence [26]. The subsequent materials reviews highlighted the basic strategies for purely organic TADF emitters [27]. This approach can also be applied to organic lasers. If triplets can be harvested instead of stored, then the same material can reduce triplet losses and contribute to gain. This strategy is not trivial because the TADF photophysics can include considerable charge-transfer component [28]. The theoretical analysis shows that efficient reverse intersystem crossing depends on more than a small singlet-triplet separation [29]. Molecular-level studies provide the explanation of how charge-transfer character can affect oscillator strength, emission width, re-absorption, and triplet removal rate [30].

Thus, the literature on TADF gain materials includes the tension between two desirable properties. Small singlet-triplet separation is favorable for delayed emission and triplet harvesting, whereas efficient radiative transition and favorable condensed-phase properties are necessary for the optical gain. Multiple-resonance TADF molecules have demonstrated efficient ultrapure blue emission due to short-range resonance [31]. The space confined charge transfer became another approach to obtain efficient and tunable luminescence [32]. The recent review of multiple-resonance emitters emphasizes the dependence of rapid reverse intersystem crossing on molecular design [33]. The computational screening has proposed a combination of the singlet-triplet energy separation and optical properties as the descriptors for gain materials [34]. The more recent computations have addressed this problem in the case of multiple-resonance TADF lasing candidates [35]. The experimental study has provided the first example of light amplification in TADF molecules [36]. Efficient electroluminescence and amplified spontaneous emission in near-infrared TADF emitters have been shown [37]. The low-threshold amplified spontaneous emission has been achieved beyond 800 nm [38]. Microring arrays have demonstrated the wavelength tunable lasing of TADF emitters [39]. The reverse intersystem crossing has become a basis for the laser generation assisted by triplet harvesting [40]. Ultrapure violet-blue emitters have demonstrated amplified spontaneous emission [41]. TADF microcrystals have produced tuneable triplet-mediated multicolor lasing [42]. The design rules for organic solid-state microlasers have been formulated [43]. The aggregation-induced emission and local excitonic character have been combined in a TADF organic laser [44]. The dedicated study of TADF gain materials has highlighted the role of triplet harvesting in lasing [45]. The more recent analysis of the optoelectronic performance has emphasized the control over triplet excitons and their utilization [46]. The above results show that the same molecular family can have different behavior in mCBP films, polymer microspheres, mCBP microplates, mCBP microrings, and neat microcrystals.

The current challenge is no longer the demonstration of TADF-based optical gain. This point has been already established. The more selective question is which emitter-states with low thresholds are most promising as a starting point for durable organic solid-state lasers when the threshold and exciton lifetime are taken into account simultaneously. A low threshold looks attractive, but the material with a long delayed component will retain an excited state population for a long time and undergo annihilation and chemical damage. Microresonator can lower the threshold, but this effect will hide poor radiative yield and triplet evacuation. Near-infrared emitter can give access to the important spectral window, but it can also exhibit a stronger non-radiative decay and high sensitivity to the host concentration. Thus, the analysis considers each material state as a photophysical-optical system rather than as a threshold value.

The goal of the analysis is the following: can TADF gain records be distinguished in terms of blue, green, red, and near-infrared operation windows using the combination of optical accessibility and fast exciton evacuation? The answer requires more than the ranking of materials. It should explain why some low-threshold records are dangerous and why some high-threshold materials are chemically sensible. The interpretation of the same photophysical variables can depend on the sample architecture. Thus, the analysis connects the numerical records of TADF gain materials in the tables with the figures illustrating the interpretation of these records from the viewpoint of material selection.

2. Photophysical Basis and Study Question

A gain material for TADF lasing must convert absorbed pump energy into stimulated emission while avoiding the accumulation of long-lived excited states. Fast prompt fluorescence describes the radiative channel of singlet excitons. Slow delayed

fluorescence describes the channel in which triplets go back to singlets through RISC. A short delayed lifetime does not necessarily mean lasing, but it is a positive feature because it means that triplets have less time to absorb light, undergo annihilation, energy transfer to impurities or other reactions. On the contrary, a long lifetime can keep photoluminescence yield high under weak pumping while becoming a problem under the higher exciton densities needed for ASE and lasing.

As the previous kinetic description must be matched with radiative yield, a high photoluminescence quantum yield shows that most of the excitations are radiative, as opposed to heat generation or chemical transformation. This is necessary for laser because there must be enough radiative cross section to compensate optical losses. However, this is not sufficient, since the threshold depends also on the waveguiding, feedback cavity, scattering, reabsorption, thickness, concentration, spectral overlap and other factors. So, while materials with high yield and long delayed lifetime can produce ASE under pulsed pumping, they can still create a dangerous level of triplet population under steady pumping. A material with low yield can produce laser in favorable microresonator, but the low yield implies that most of the excitations have nonradiative fate.

The effective separation between triplet harvesting and ground state, called here ΔE_{eff}, constitutes the third key element. Small separations help thermally-assisted upconversion in general, but spin-vibronic coupling can influence efficiency of this process [47]. According to TADF theoretical framework, state structure and their coupling must be considered at the same time [29]. Molecular approach also shows that the correlation cannot be determined only by the energy separation [30]. In some cases, efficient RISC occurs via higher triplet states or via mixing of local-excited and charge-transfer states. But in other cases, small separation between states results in low oscillator strength, because of the charge-transfer nature. Therefore, for the laser choice, ΔE_{eff} is just a penalty term, not an independent variable. This parameter helps to find systems with energetically demanding triplet recovery, but it cannot substitute experimental determination of threshold, yield and lifetime.

The condensed phase state of the system constitutes the fourth pillar of the analysis. Host-diluted mCBP films can be useful, because dilution suppresses concentration quenching and isolates the emitter. Microplates and microring can provide geometry-related feedback and mode confinement. Self-assembled neat microcrystals can give high oscillator density and resonators. They are also more sensitive to the packing defects and to the aggregation. Theory of H- and J-aggregates describes the reasons of this effect [48]. Aggregation-induced luminescence offers the opposite example of how condensed-phase packing can enhance rather than suppress luminescence [49]. Polymer microsphere also constitutes an optical feedback system, but due to polymer dilution and scattering, the threshold can be very high. Such states should not be combined into a single molecular variable because the material showing good properties in one state can lose them in another.

The gain wavelength and fluorescence wavelength are considered separately. Fluorescence wavelength characterizes the dominant spontaneous emission under described conditions. Gain wavelength characterizes the part of spectrum where ASE or lasing occurs. The difference between two quantities can be harmless due to feedback selecting narrower part of spectrum, but it can also imply reabsorption, cavity selection, aggregate emission, or morphology-dependent spectral shift. The records cover the spectrum from the blue film ASE around 448-494 nm up to the near-infrared ASE or lasing above 740 nm. Thus, such spectral range makes possible examination of the same selection criteria under different constraints on nonradiative and optical losses.

The reliable comparison must therefore answer three connected questions. The first one is which entries achieve low threshold without using long-lived delayed state. The second question is which structures use molecular photophysics to produce the feedback without masking low yield or inefficient exciton removal. And the third one is which spectra are still credible taking these penalties into account. The analysis answers to those questions by computing an integrated score while keeping all variables in tables and plots accessible.

3. Dataset and Analysis Technique

3.1 Emitter-state Variables

The dataset consists of sixteen emitter-state observations. The definition of each observation is based on compound identity and condensed state since the same compound can have varying properties with respect to the gain process in different configurations such as films, microplates, microrings, microspheres, and microcrystals. Each observation consists of the following data: the compound name, sample design, gain process, fluorescence wavelength, gain wavelength, prompt and delayed lifetime, photoluminescence quantum efficiency, effective separation between the triplet and harvesting state, and optical threshold. In cases where an optical threshold was reported as a range of values, the entire range is kept in the table with the lower limit being used to calculate the utility score since it indicates the best-known operation point for the particular material state. Entries not having lifetime values are still included in the spectral and threshold analysis, although penalized in lifetime-based ranking since fast exciton decay cannot be deduced without lifetime value.

Table 1: TADF gain records.

ID	Compound	Architecture	Process	λ_{FL} (nm)	λ_{gain} (nm)	τ_{p} (ns)	τ_{d} (μs)	Φ_{PL}	ΔE_{eff} (eV)	P_{th} (μJ cm^{-2})
1	1a	mCBP film	ASE	460	460	8.8	93.7	0.80	0.18	2.8
2	1a	mCBP microplate	lasing	460	480	8.8	93.7	0.80	0.18	5.5
3	1b	mCBP film	ASE	469	494	6.0	65.3	0.90	0.14	1.6
4	2a	mCBP film	ASE	454	468	4.0	0.8	0.93	0.28	3.3
5	2b	mCBP film	ASE	430	448	5.4	0.3	0.90	0.27	12.0
6	3	PS microsphere	lasing	520	563	10.7	1.4	0.71	0.06	84–95
7	3	mCBP microplate	lasing	560	567	11.2	1.8	0.43	0.02	30.5
8	4a	microcrystal	lasing	502	525	10.5	3.5	0.65	0.19	3.5
9	4b	microcrystal	lasing	532	561	9.7	2.0	0.80	0.02	5.0
10	4c	microcrystal	lasing	580	650	5.5	9.9	0.70	0.12	3.0
11	4d	microcrystal	lasing	560	560	0.8	0.9	0.12	0.12	10.6
12	5	microcrystal	ASE	610	610	2.3	3.8	0.17	0.24	23.6
13	6	mCBP microring	lasing	653	677–700	1.3	191	0.13	0.26	4.0
14	7	mCBP film	ASE	706–782	738–798	2.3	28	0.70	0.37	4.7–36.7
15	7	mCBP microplate	lasing	721	740	2.3	28	0.70	0.37	3.6
16	8	mCBP film	ASE	760–801	801–860	–	–	0.45	0.30	7.5–91.3

The values in Table 1 explain why such comparison cannot be reduced to one single parameter. The threshold range extends from 1.6 μJ cm^{-2} for 1b in an mCBP film to 84–95 μJ cm^{-2} for compound 3 in PS microspheres. Delayed lifetimes extend from 0.3 μs for 2b to 191 μs for compound 6 in mCBP microrings. Photoluminescence quantum yield extends from 0.12 for 4d and 0.13 for 6 to 0.93 for 2a. All these ranges are greater than the usual spread of experimental error and suggest real differences in emitter-host-resonator interaction.

ID	Architecture	Mode	λ_{gain} (nm)	P_{th}	τ_d	Φ_{PL}	ΔE_{eff}
1a	film	ASE	460	2.8	93.7	0.80	0.18
1a	microplate	lasing	480	5.5	93.7	0.80	0.18
1b	film	ASE	494	1.6	65.3	0.90	0.14
2a	film	ASE	468	3.3	0.8	0.93	0.28
2b	film	ASE	448	12.0	0.3	0.90	0.27
3	PS microsphere	lasing	563	84--95	1.4	0.71	0.06
3	microplate	lasing	567	30.5	1.8	0.43	0.02
4a	microcrystal	lasing	525	3.5	3.5	0.65	0.19
4b	microcrystal	lasing	561	5.0	2	0.80	0.02
4c	microcrystal	lasing	650	3.0	9.9	0.70	0.12
4d	microcrystal	lasing	560	10.6	0.9	0.12	0.12
5	microcrystal	ASE	610	23.6	3.8	0.17	0.24
6	microring	lasing	677--700	4.0	191	0.13	0.26
7	film	ASE	738--798	4.7--36.7	28	0.70	0.37
7	microplate	lasing	740	3.6	28	0.70	0.37
8	film	ASE	801--860	7.5--91.3	--	0.45	0.30

Figure 1: Emitter-state records.

Moreover, the list reveals that there exist many pairs of apparently good values accompanied by severe penalties. The low threshold and yield of 0.90 characteristic of compound 1b correspond to a long-lived excited state with 65.3 μs lifetime. Similarly, compound 6 has a low microring threshold of 4.0 μJ cm^{-2} and an unacceptably low yield of 0.13 and delayed lifetime of 191 μs. Compound 4d has fast decay rates of both prompt and delayed emission but very low yield of 0.12. It suggests inefficient gain and a high risk of energy losses through nonradiative transitions. This list thus allows a holistic approach where the numerical values are kept intact while interactions between variables are illustrated.

The emitter-state summary in Figure 1 provides the visual record of the data used throughout the manuscript. Every plot corresponds to the respective condensed phase in which the measurements have been done and not just molecular structure itself. It prevents film, microplate, microsphere, microring and microcrystal records from being considered as various versions of the same sample. It is important for the current study because low threshold in a resonator state and low threshold in a film of host-diluted molecules mean different things regarding exciton density, optical feedback and repeated pump survival.

3.2 Optical utility of exciton evacuation

The comparative utility is expressed as a transparency ranking value rather than an immutable law of physics. It gives credit to radiative efficiency and low excitation threshold since these two factors determine the most fundamental aspect of optical

utility. It also awards short delayed lifetime, short prompt lifetime, and reduced effective triplet harvesting separation since these factors decrease the expense of exciton evacuation. This utility value is termed the optical utility of exciton evacuation and defined as

$$U_{\mathrm{EO}} = 100\,[0.30\Phi_{\mathrm{PL}} + 0.25\Theta + 0.20E_d + 0.15E_g + 0.10E_p]\,, \tag{1}$$

where

$$\begin{aligned} \Theta &= \exp(-P_{\mathrm{th}}/20), & E_d &= \exp(-\tau_{\mathrm{d}}/25), \\ E_g &= \exp(-\Delta E_{\mathrm{eff}}/0.25), & E_p &= \exp(-\tau_{\mathrm{p}}/10). \end{aligned} \tag{2}$$

The constants of Eq. (2) establish a realistic scale for the sixteen-compound dataset. The 20 μJ cm^{-2} threshold is considered a considerable cost but not a catastrophic failure since some of the resonance structures can carry meaningful information despite being in that range. The delayed lifetime of 25 μs is considered a significant retention time under repeated excitations. The triplet-harvesting energy gap of 0.25 eV is considered a significant energetic cost of thermally-assisted recovery. The given constants do not claim universality. They provide a uniform comparison within the dataset and enable a consistent inspection of the ranking in view of the provided values.

The weights assign the maximum to photoluminescence yield since radiative efficiency is the most straightforward indication of efficient exciton-photon conversion on a material level. Threshold is assigned the second highest weight since a laser active medium needs to reach gain at a realistic fluence level. Delayed lifetime is assigned a significant but not dominating weight since it is a risk factor, not a lifetime measure per se. Energy-gap and prompt-lifetime terms improve the ranking by penalizing energetically costly recovery and slow prompt cycling. The given ranking scheme differs from both the threshold-only ranking and the purely photophysical one since it considers the question of optical accessibility and kinetic suitability of an emitter state simultaneously.

The absence of the delayed lifetime cannot be treated as a low-risk value for the given purposes. That is why the lifetime-related term is assumed to be zero in case of lacking data on the delayed lifetime. Such conservative approach influences compound 8 which is still of great importance as a near-infrared ASE record but which cannot be included into the ranking of strong exciton evacuation candidates without prompt and delayed lifetimes.

4. Results and Discussion

4.1 Spectral accessibility and threshold distribution

The spectral threshold landscape of Figure 2 proves that the data set is not comprised of just one narrow family of optically accessible TADF gain media. The data spans all the way from the blue films at 448–494 nm to the near-infrared ASE of 801–860 nm. At the same time, the lowest values of the thresholds correspond to several distinct sample forms. For example, the compound 1b shows the lowest threshold at 1.6 μJ cm^{-2} in the mCBP film, compound 2a achieves the blue ASE at 468 nm and $P_{\mathrm{th}} = 3.3$ μJ cm^{-2}, compound 4c exhibits the red laser emission at 650 nm with $P_{\mathrm{th}} = 3.0$ μJ cm^{-2}, while compound 7 demonstrates the near-infrared plate lasing at 740 nm with $P_{\mathrm{th}} = 3.6$ μJ cm^{-2}. Both horizontal and vertical error bars indicate the range of thresholds and wavelength, respectively, for records like compound 7 and 8 to allow a distinction between a single operating point and the range dependent on concentration/wavelength.

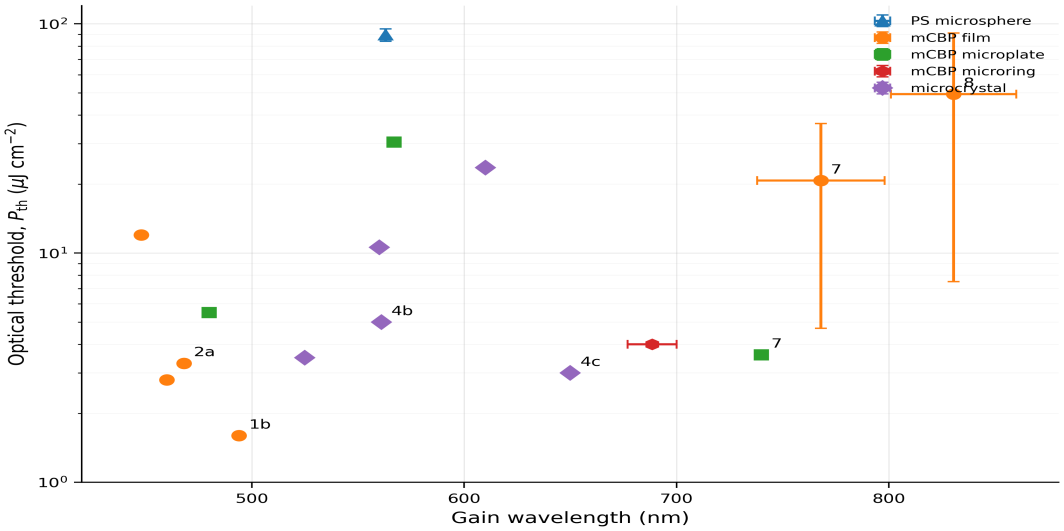

Figure 2: Spectral threshold landscape.

The location of the blue film data proves that the donor-acceptor type of emitters can provide the low ASE threshold only if the host material provides an efficient radiative output. At the same time, the red and near-infrared points are just as important because they prove that the accessible thresholds are not limited to the high-energy part of the spectrum. The near-infrared film data of compound 8 shows the wide range of the threshold from 7.5 to 91.3 μJ cm^{-2} and a wide gain range of 801–860 nm that makes it spectrally very valuable but not very informative in regard to the stability.

The yield vs threshold comparison in Fig. 3 introduces an additional criterion to the threshold space. The interesting area for this case corresponds to the lower right part of the figure; it consists of materials with low threshold values and high quantum yield of photoluminescence. Compound 2a occupies the most favorable position here, providing $\Phi_{PL} = 0.93$ and $P_{th} = 3.3$ μJ cm^{-2}. Also compound 1b fits well into this category with $\Phi_{PL} = 0.90$ and $P_{th} = 1.6$ μJ cm^{-2}. In turn, compound 6 features a low microring threshold value of 4.0 μJ cm^{-2} and $\Phi_{PL} = 0.13$, whereas compound 4d has fast decay but low yield 0.12. These two cases demonstrate that resonator assistance or rapid decay is not enough when the radiative probability is weak.

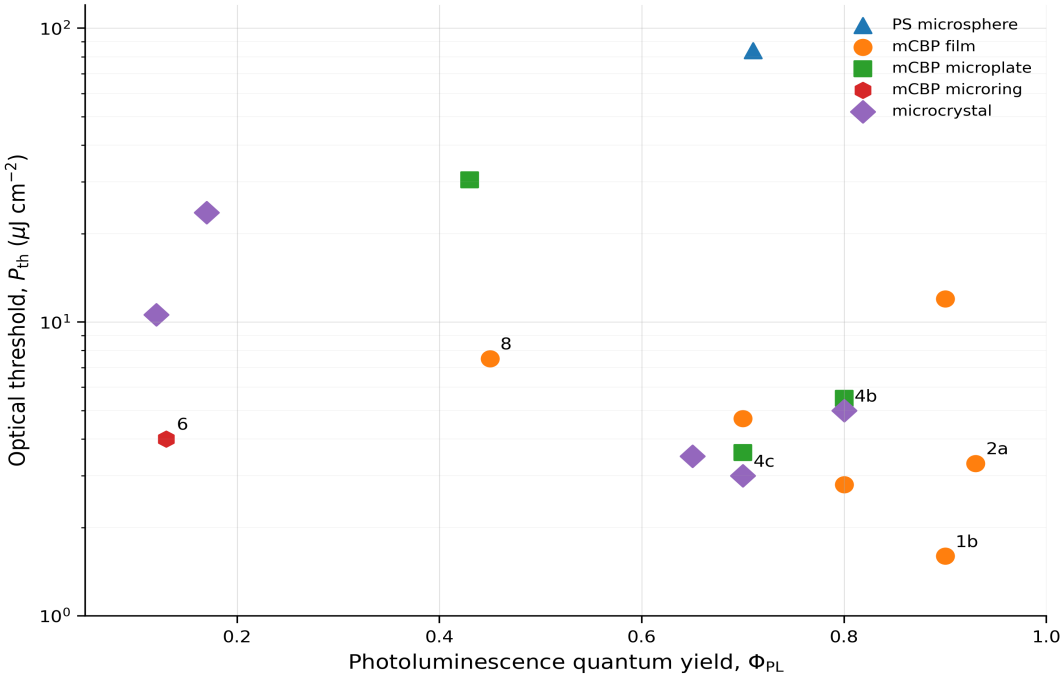

Figure 3: Yield-threshold window.

Comparison also explains the reason behind the differences between the polymer microsphere and microplate states with respect to the compound 3. In the PS microsphere state, the yield is relatively moderate at 0.71, but the threshold is quite high at 84-95 μJ cm^{-2}. On the other hand, in the mCBP microplate state, the threshold becomes relatively low at 30.5 μJ cm^{-2}, but the yield becomes low at 0.43. Thus, the compound still remains useful because it separates the photophysical prospects from the optical realization of a material. Development of materials will certainly enhance this record either by lowering the optical losses or changing the feedback state; however, the current state cannot be deemed to be threshold efficient lead.

4.2 Exciton retention relative to optical demand

The lifetime-threshold window in Fig.4 is the key diagnostic plot of the whole manuscript since it directly checks whether a low-threshold state provides the fast evacuation of delayed excitons. The record compound 2a belongs to the low-threshold and short-delay domain; its threshold is $P_{th} = 3.3$ μJ cm^{-2}, and the delayed lifetime equals $\tau_d = 0.8$ μs. Another favorable compound 4b has a microring lasing threshold equal to 5.0 μJ cm^{-2} and a delayed lifetime equal to 2.0 μs. The compound 4c is also promising for the red window; it has a relatively low threshold, but a more prolonged delayed lifetime of 9.9 μs.

The contrast between 1b and 2a helps to understand why the paper does not rank compounds based on the threshold value. The compound 1b has the lowest threshold in films, but the delayed lifetime is 65.3 μs. In other words, such an extensive time scale implies the presence of an appreciable excited-state population after the prompt emission decay. Although this comparison cannot prove the operability failure of 1b because there are no experimental lifetime data in a pump cycle, it shows the elevated retention risk compared to 2a. The compound 6 represents even a stronger warning sign since it has a low microring threshold together with the delayed lifetime of $\tau_d = 191$ μs and low yield.

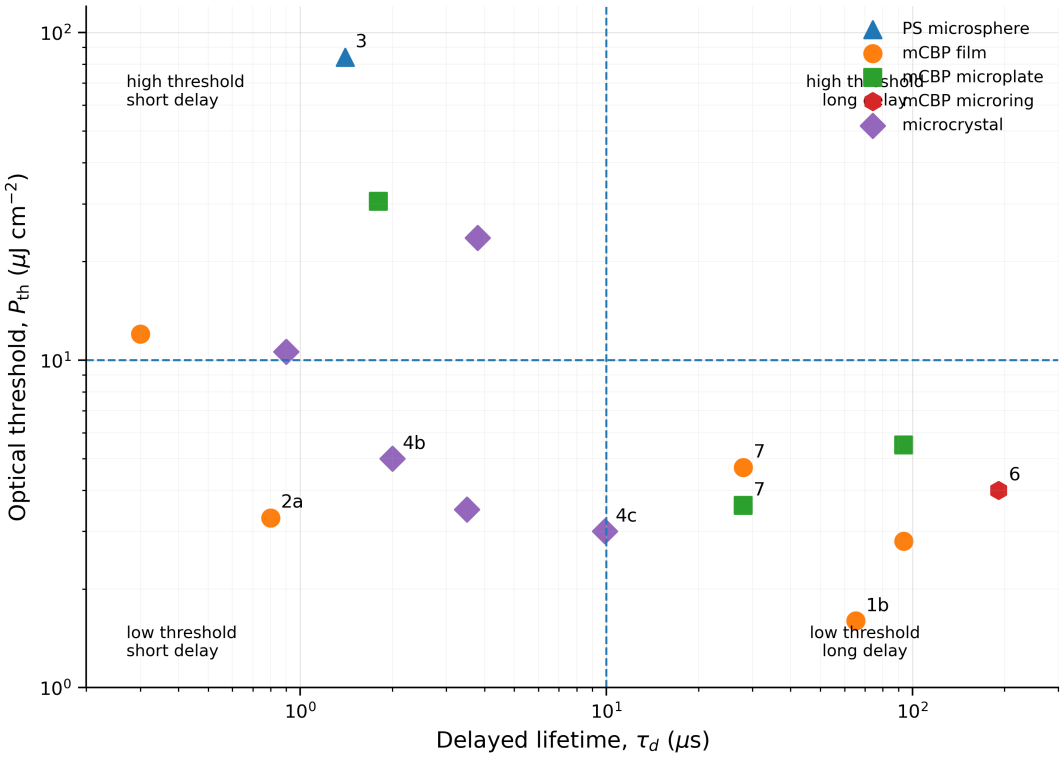

Figure 4: Lifetime-threshold window.

The high-threshold and short-delay region includes the records which cannot be considered chemically poor. The compound 2b has the delayed lifetime equal to 0.3 μs and the yield of 0.90 but its ASE threshold is rather large – 12.0 μJ cm^{-2}. The compound 3 in PS microspheres has a shorter delayed lifetime (1.4 μs) and a higher PLQY of 0.71 but the threshold is rather high as well. These records mean that rapid exciton evacuation can be realized in material states requiring further improvement in confinement, optical loss, or host material. The lifetime-threshold plot thus divides the dataset into the types of design issues.

Table 2: Architecture-level summaries.

Architecture family	Records	Best P_{th} (μJ cm^{-2})	Median P_{th} (μJ cm^{-2})	Median τ_d (μs)	Median Φ_{PL}
Host-diluted film	6	1.6	4.0	28.0	0.85
Host microplate	3	3.6	5.5	28.0	0.70
Neat microcrystal	5	3.0	5.0	3.5	0.65
Polymer microsphere	1	84	84	1.4	0.71
Host microring	1	4.0	4.0	191	0.13

From the architectural summary table (Table 2), it is evident that a change in state of the sample will alter the interpretation of all the numbers. While the host-diluted films have the best absolute threshold and high median yield, their median delayed lifetime will be higher because of the existence of the long-living 1a, 1b, and 7. On the other hand, neat microcrystals will exhibit low median delayed lifetime and high threshold range, though they depend on the quality of the crystals and the concentration of defects. The host microplates are useful for feedback and near-infrared accessibility, while the median delayed lifetime is still moderate.

4.3 Architecture-level performance profiles

The architecture threshold profile in Figure 5 splits the operating states into their physical families. Host-diluted films represent the most extensive family in the data set and also include the lowest-threshold record; however, their spread includes also high-threshold near-infrared operation. Neat microcrystals belong to a compact and competitive family, which consists of several few-μJ cm^{-2} thresholds. Host microplates demonstrate the impact of feedback on lowering threshold of selected emitters, especially the near-infrared compound 7. One-record families of a microsphere and microring must be analyzed carefully since there is only one physical state for each architecture; yet, they are useful diagnostic extremes.

The threshold profile illustrates why architecture cannot be described categorically. A microcrystal is not necessarily better than a film; a microring is not necessarily more stable just because it is a resonator. The case of compound 6 shows that the emitter can provide low threshold while being weak by delayed lifetime and yield. Conversely, compound 3 in the

PS microsphere demonstrates poor lifetime and high threshold even though its kinetic profile is favorable. Thus, architecture selection is possible after evaluation of the emitter's optical and kinetic characteristics.

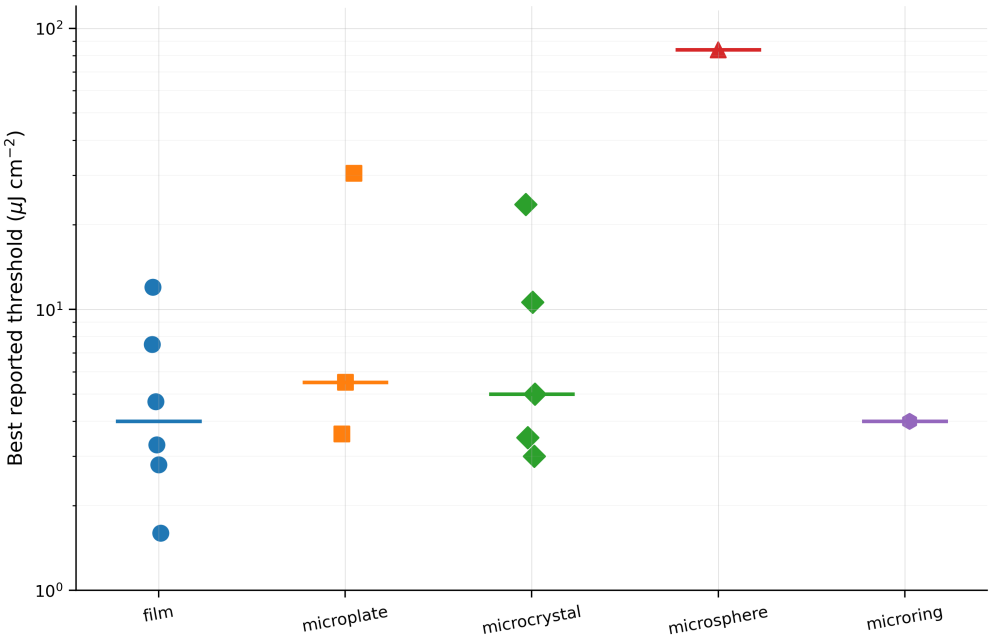

Figure 5: Architecture threshold profile.

The architecture lifetime profile in Figure 6 complements the threshold profile by demonstrating the duration of delayed states' life in each physical family. Neat microcrystals are favorable from median delayed lifetime point of view since compounds 4a–4d and 5 mostly demonstrate less than 10 μs. The host films' family is more diverse: compound 2a and 2b evacuate delayed states quickly; however, 1a and 1b maintain delayed population up to tens of microseconds. Microplate family inherits such diversity since it includes fast compound 3 and also near-infrared compound 7 with delayed lifetime.

The combination of threshold and lifetime profiles in Figures 5 and 6 leads to a useful conclusion. Morphology improves the emitter only in case of selection of the state, which decreases optical losses without creation or maintaining of damaging excited-state reservoir. Neat microcrystals appear to be promising platform for green and red lasing due to moderate thresholds and acceptable delayed lifetimes in the 4-series compounds. Host films are good platform for blue emitters when molecules are characterized by fast delayed emission, e.g., 2a and 2b. Near-infrared microplates are still valuable but require reduction of delayed retention for becoming more reliable durability-oriented candidates.

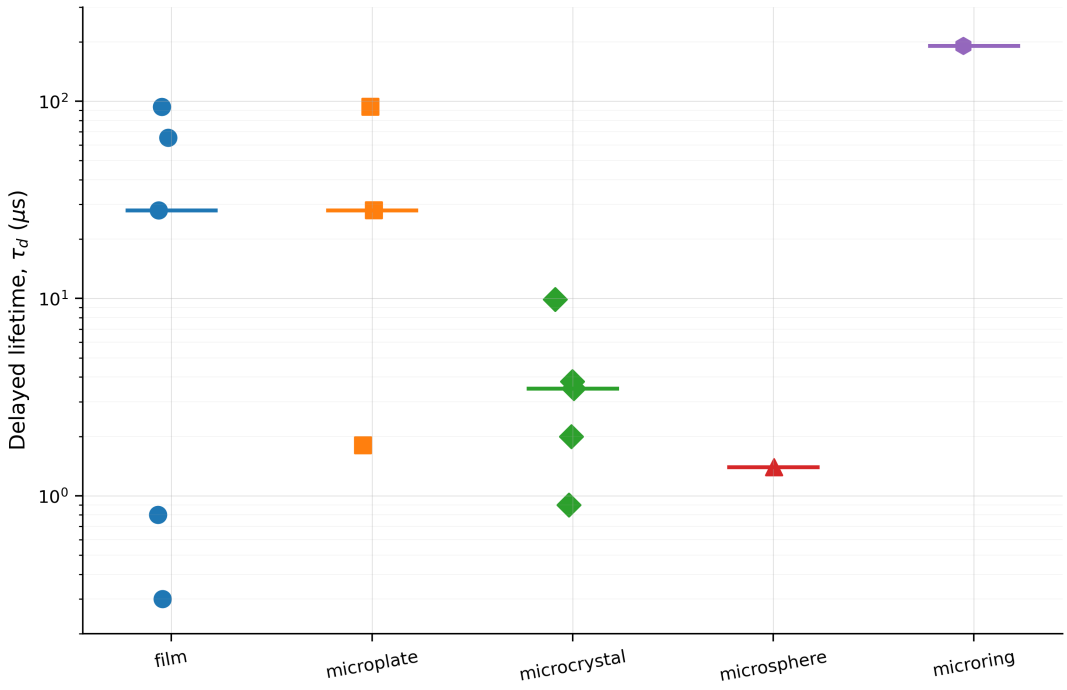

Figure 6: Architecture lifetime profile.

4.4 Utility Ranking and Material-State Profiles

The integrated utility ranking in Figure 7 integrates the metrics of threshold accessibility, radiative yield, prompt lifetime, delayed lifetime, and effective energy separation into a single ranking. 2a is the top film record since it exhibits high yield, low threshold, short prompt decay, and short delayed emission. 4b is the top green microcrystal record since it features small effective singlet-triplet separation of 0.02 eV, high yield, short delayed lifetime, and low lasing threshold. 4c is a highly ranked record due to its ability to provide red lasing with low threshold in spite of its relatively long delayed lifetime.

The ranking has two key implications. First, the ranking does not simply reflect the lowest thresholds. Record 1b still ranks among the top records despite its low threshold and yield due to its 65.3 μs delayed lifetime. Second, some of the low-threshold states change positions when kinetics information is used. Record 6 does not become a lead record in spite of its microring threshold due to unfavorable yield and delayed lifetime. In other words, the ranking works as designed, favoring material states where lasing threshold is low and exciton is cleared rapidly.

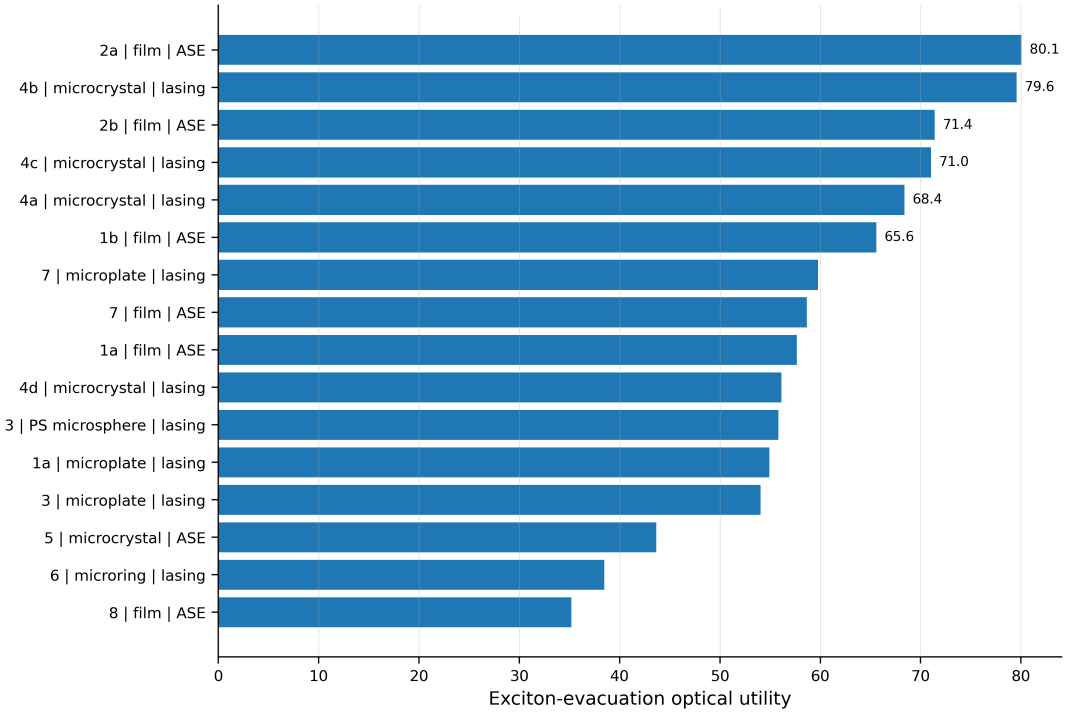

Figure 7: Integrated utility ranking.

The normalized performance profiles in Figure 8 explain the above ranking in greater detail. Record 2a features balanced values for all four positive metrics, while record 4b exhibits good values for energy separation and yield at acceptable threshold and lifetime values. Record 1b features strong threshold and yield metrics but low delayed-lifetime metric. Record 6 features weak yield and delayed-lifetime metrics and a strong threshold metric. Record 7 is an important one as it provides near-infrared lasing but it is far from being balanced in terms of energy separation and delayed lifetime metrics.

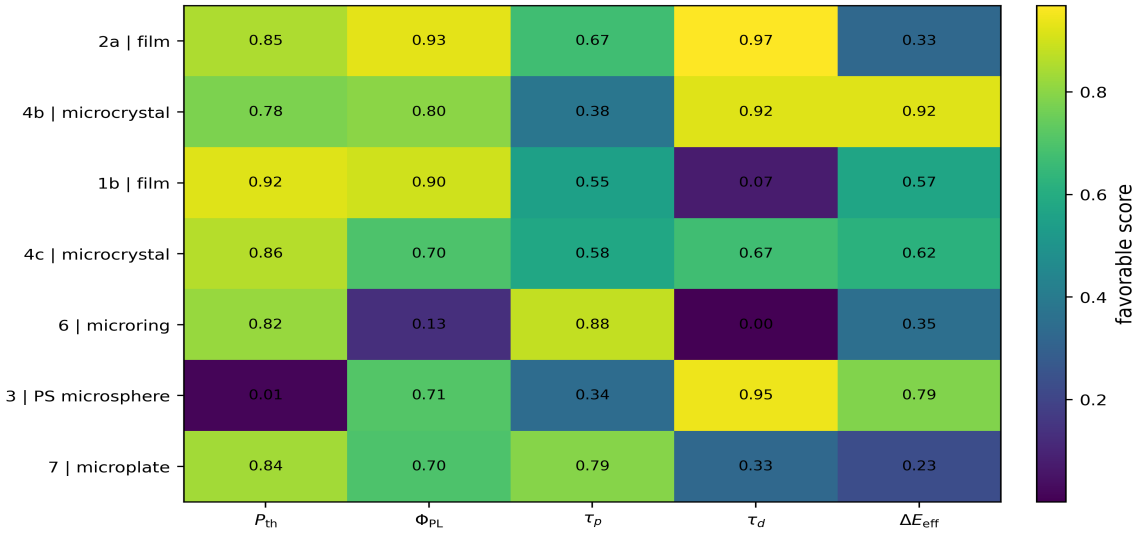

Figure 8: Performance profiles.

The usefulness of the profile view is that it determines what needs to be enhanced in each compound. The 2b compound needs lowering of the threshold value rather than the rapid exit of the exciton. For compound 3 in PS microspheres, there is need to enhance optics instead of changing the kinetics of delayed states. In the case of compound 4c, the delay tail needs to be inhibited but the red microcrystal lasing needs to be retained.

4.5 Energy separation among color targets

The energy separation plot in Figure 9 displays ΔE_{eff} against gain wavelength and marker size correlated with accessibility of threshold. Minimum effective separations are achieved by compound 3 in mCBP microplates and compound 4b in microcrystals, both at 0.02 eV. Their thresholds are vastly different: compound 4b achieves lasing in microcrystals at 5.0 μJ cm^{-2}, whereas compound 3 in mCBP microplates needs 30.5 μJ cm^{-2}.

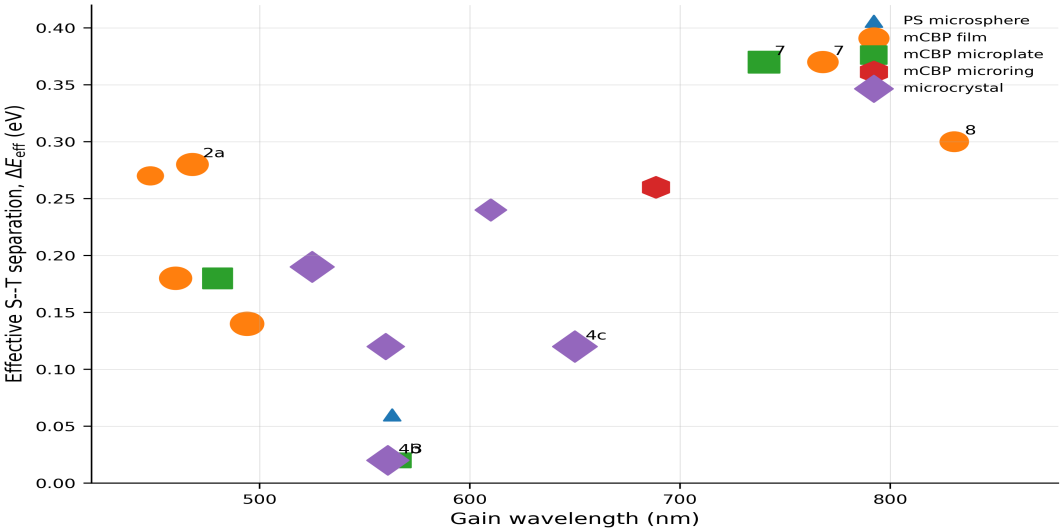

Figure 9: Energy separation range.

The blue film records represent an opposite example. While compound 2a possesses bigger effective separation than 1b, it remains the better balanced lead since the delayed lifetime is short and the yield is high. The red and near-infrared records provide one more limitation: compound 4c achieves 650 nm lasing with $\Delta E_{\text{eff}} = 0.12$ eV and low threshold, compound 7 reaches 740 nm lasing with $\Delta E_{\text{eff}} = 0.37$ eV. Compound 8 expands the ASE range up to 801–860 nm, but lack of prompt and delayed lifetimes makes difficult interpretation of triplet treatment in that system. It demonstrates that energy separation has to be considered together with other experimental data on kinetic and optical threshold.

4.6 Lead states specific for windows

The lead selection summarized in Table 3 makes clear that the ranking can be used for choosing wavelength-specific material candidates. Blue film device has to give preference to 2a if balanced threshold, yield and exciton extraction are necessary, whereas 1b remains the least threshold competitor. The green microcrystal program has to start with 4b as the best studied material in this architectural class. The red microcrystal program should consider 4c as the strong lead and try to reduce delayed-lifetime penalty. The near-infrared program should make a difference between the microplate record of 7 and the farther-red film record of 8, since spectral shift without lifetime information does not solve degradation problem.

Table 3: Candidate windows.

Operating window	Record	Architecture	Gain (nm)	P_{th} (μJ cm^{-2})	τ_{d} (μs)	Main concern
Balanced blue film	2a	mCBP film ASE	468	3.3	0.8	no dominant penalty
Threshold comparator	1b	mCBP film ASE	494	1.6	65.3	slow delayed tail
Green microcrystal	4b	neat microcrystal lasing	561	5.0	2.0	crystal control
Red microcrystal	4c	neat microcrystal lasing	650	3.0	9.9	moderate retention
Near-infrared plate	7	mCBP microplate lasing	740	3.6	28	concentration control
Far-red/NIR film	8	mCBP film ASE	801–860	7.5–91.3	–	missing lifetime

This can be seen clearly in the window lead-state diagram of Figure 10. The lead state varies with wavelength: 2a is the lead for the balanced blue film window, 4b is the lead for the green microcrystal window, 4c is the lead for the red microcrystal window, and 7 is the lead for the most comprehensive near-infrared lasing window. Compound 8 has been left out of the discussion as a lead state since the lifetimes have not been reported. It is crucial in understanding the paper since this prevents the record of the longest wavelength from being unduly praised due to its broad spectrum coverage.

The combination of information in Figures 2–10 provides an answer to the material selection problem based on emitter states. TADF gain records can be categorized into useful operating windows only when the threshold, yield, delayed lifetime, energy separation, and morphology are taken into consideration at the same time. Threshold needs to be low, but it will be convincing only if high radiative yield and rapid exciton removal take place. The most promising compounds in this database are therefore not those with the most extreme value for any single property but rather those where all the major constraints are met.

Window	Lead	State	λ_{gain}	P_{th}	τ_d	Φ_{PL}	ΔE_{eff}
Blue	2a	mCBP film ASE	468	3.3	0.8	0.93	0.28
Green	4b	microcrystal lasing	561	5.0	2.0	0.80	0.02
Red	4c	microcrystal lasing	650	3.0	9.9	0.70	0.12
Near-IR	7	mCBP microplate lasing	740	3.6	28	0.70	0.37
Far-IR comparator	8	mCBP film ASE	801--860	7.5--91.3	--	0.45	0.30

Figure 10: Window lead states.

5. Implications for TADF Laser Materials Design

The first implication is that the design of a TADF laser material should move from the report of isolated thresholds to the combined reporting of thresholds and exciton evacuation. Threshold gives us the information about the ability of reaching gain with the particular optical setup. Delayed lifetime reflects the amount of time which is required to evacuate a substantial number of excitations from the system in the recovered or recoverable reservoir. Photoluminescence yield shows whether these excitations are radiative or non-radiative. It should be mandatory to provide this data in the same condensed phase whenever possible to get a comprehensive picture of material potentialities. The lack of any of this variable means that the judgment about the durability is weakened.

In the case of blue and blue-green films, the most urgent design target is not just lowering the threshold. There are film entries which have the thresholds around a few microjoules per square centimeter already. The harder goal is to keep the delayed lifetime low while maintaining the high yield and low spectral overlap. Compound 2a proves that such a combination is possible. Compound 1b proves that the minimum threshold may be less significant when the delayed lifetime is high. In this case, molecular strategies that increase the RISC rate while keeping high oscillator strength are more valuable than those that decrease the threshold by increasing the retention of excitations.

In the case of neat microcrystals, we see that the packing may be advantageous if it supports the feedback process and the radiative emission. Compound 4b is the successful case because its small separation, high yield, and low delayed lifetime are good fit to microcrystal resonator. Compound 4c is the extension of this idea into the area of red lasing but introduces the longer delayed lifetime. Microcrystal design should therefore focus on reproducible packing, defect control, and packing motifs which are capable of preserving cavity quality without creating quenching. Even small changes in the crystal habit or impurity concentration can affect the balance between the radiative gain and exciton loss.

Near-infrared TADF gain media are even harder cases. The long wavelengths mean not only reduced energy gap but also higher tendency to nonradiative decay because of the energy-gap law. However, the values for compounds 7 and 8 prove that there are still meaningful gains in the near-infrared. Compound 7 in the mCBP microplate is the more complete lead because both threshold and lifetime are known. Compound 8 extends into the near-infrared but has no prompt and delayed lifetime data in the table. Thus, the consequence of design is that the near-infrared claims should be supported by time-resolved experiments and concentration dependence threshold measurements because spectral extension may hide growing loss channel.

The results also point to the role of host material. We can see that mCBP is used in many entries because it provides high triplet level medium for the emitter dilution. Host may provide reduction of aggregation, control of energy transfer processes, and tuning of local dielectric environment. Host may create the additional losses if there are improper triplet level, exciton diffusion or concentration. The comparison of the film and microplate records proves that the host-controlled architecture improves feedback, however, the emitter's kinetic signature stays visible. Therefore, host engineering should be judged by its ability to lower threshold and shorten the effective lifetime of the delayed emission.

The role of resonator geometry should also be considered carefully. Resonator may help to decrease the threshold by providing more feedback or more mode confinement. This may be good if the material has high yield and fast exciton cycling but may be undesirable if the resonator compensates for the poor material quality because the low threshold may not guarantee the operational stability. Compound 6 is the case to prove this point. The threshold of this compound in

microring is low but the photophysical parameters show low radiative efficiency and long delayed lifetime. Device engineers should not take the low threshold provided by the resonator as the evidence of the durable gain without kinetic data.

All these implications follow the general trend from OLED materials to the laser materials. OLED may tolerate the delayed emission because there is continuous generation of excitons in lower concentrations and the efficiency roll-off is controllable. Laser requires intensive population inversion or high gain density so that the delayed emission channel may become the source of benefit through triplet harvesting or loss through the retention of excitons. Thus, the design task is to increase the RISC rate enough to make TADF assist gain but not leave slow excited-state channel.

6. Analytical Boundaries and Reproducibility

All of the numerical data provided in Table 1 is kept, and there is never any substitution of a missing value with any preferable value. The score is cautious with the missing lifetime data since a stability-focused comparison cannot assign a benefit to the kinetic parameter not reported. Range is kept in threshold values instead of collapse of the range. This is crucial in near-infrared films because the ranges of the concentrations- or wavelengths-dependent thresholds may vary greatly. The smallest threshold value is assigned the score in the consideration because it is the best-proven condition, but the range is discussed to prevent the reader from confusing a best case with a universal property.

A number of limitations should be acknowledged. The delayed fluorescence lifetime serves as a measure of exciton retention, not a measure of the chemical lifetime during laser operation. Degradation relies on oxygen, impurities, pump repetition rate, local heating, photoproduct formation, host stability, exciton diffusion, resonator geometry, and encapsulation. The score cannot account for spectral linewidth, stimulated-emission cross section, gain coefficient, modal loss, or absolute photobleaching rate since these parameters are not known for all records. The ranking process is thus a cautious comparison of incomplete records rather than a replacement for device testing.

The assignment of the exponential penalty involves some choice as well. The exponential terms are adequate to make the extremely long lifetimes and the extremely high thresholds progressively less advantageous, but another research group can assign other values of the constants depending on a certain pump repetition rate or device geometry. The conclusion about the fact that 2a, 4b, 4c, and 7 provide the best window-specific records is reliable since it can be seen both in the tabulated values and in the score. The precise spacing between the middle-ranked records should be considered approximately.

The reproducibility of the comparison is based on the transparency of the variables and equations. All of the values used in the computation are presented in Table 1. The score in Eq. (1) includes only the values and the constants described in Eq. (2). Figures illustrate the same dataset from various perspectives without involving any new measurements. The equation can be reweighted for a different application. E.g., the near-infrared sensing project can prioritize the gain wavelength while the electrically pumped laser project can enhance the delayed-lifetime penalty.

A complete set of records would include the operational half-life during the repeated pulse excitation, the transient absorption at the gain wavelength, the triplet absorption spectra, the gain coefficients, the linewidths, the pump repetition rates, the concentration series of the host, and the morphology statistics. Such records would enable the score to transition from proxy-based selection to the stability calculation. Until complete records become available, the current analysis offers a disciplined approach to avoid any overinterpretation of the threshold alone.

7. Conclusion

The central problem was whether TADF gain records can be divided into practically operating windows using the combination of optical threshold with exciton evacuation, radiative yield, energy separation, and condensed-phase architecture. The answer is positive. The comprehensive analysis reveals that the most promising candidates are not simply the lowest-threshold records. Record 2a in the mCBP film is the most credible balanced film record since it possesses the highest yield, the lowest threshold, and the sub-microsecond delayed emission. Record 4b is the most promising green microcrystal record since it combines the small effective triplet-harvesting separation, the high yield, the short delayed lifetime, and the moderate lasing threshold. Record 4c is the most promising red microcrystal record, and record 7 in the mCBP microplates is the most credible near-infrared lasing window.

The comparison highlights also the reasons for several promising records requiring some caution. Record 1b is the threshold leader among the film records, but its delayed lifetime is too long to be treated as the most durable choice. Record 6 reveals that the feedback of the resonator can provide the low threshold even when the yield and the delayed lifetime are poor. Record 8 extends the near-infrared ASE window, but the missing lifetime data prevent from establishing the stability ranking. These differences provide the answer to the research question: a TADF gain medium should be chosen as an emitter-state record in which threshold, yield, exciton evacuation, and morphology are favorable. Thus, the optimal

route towards durable organic solid-state lasers is not the threshold minimization, but the design of the condensed-phase system that efficiently evacuates triplets while providing the radiative gain.

Conflict of Interest

The author declares no competing financial or personal interests.

References

[1] Maiman, T. H. (1960). Stimulated optical radiation in ruby. nature, 187(4736), 493-494.
[2] Sorokin, P. P., & Lankard, J. R. (1966). Stimulated emission observed from an organic dye, chloro-aluminum phthalocyanine. IBM Journal of Research and Development, 10(2), 162-163.
[3] Soffer, B. H., & McFarland, B. B. (1967). Continuously tunable, narrow-band organic dye lasers. Applied physics letters, 10(10), 266-267.
[4] Hide, F., Diaz-Garcia, M. A., Schwartz, B. J., Andersson, M. R., Pei, Q., & Heeger, A. J. (1996). Semiconducting polymers: a new class of solid-state laser materials. Science, 273(5283), 1833-1836.
[5] Tessler, N., Denton, G. J., & Friend, R. H. (1996). Lasing from conjugated-polymer microcavities. Nature, 382(6593), 695-697.
[6] Kozlov, V. G., Bulović, V., Burrows, P. E., & Forrest, S. R. (1997). Laser action in organic semiconductor waveguide and double-heterostructure devices. Nature, 389(6649), 362-364.
[7] McGehee, M. D., & Heeger, A. J. (2000). Semiconducting (conjugated) polymers as materials for solid-state lasers. Advanced Materials, 12(22), 1655-1668.
[8] Scherf, U., Riechel, S., Lemmer, U., & Mahrt, R. F. (2001). Conjugated polymers: lasing and stimulated emission. Current Opinion in Solid State and Materials Science, 5(2-3), 143-154.
[9] Samuel, I. D. W., & Turnbull, G. A. (2007). Organic semiconductor lasers. Chemical reviews, 107(4), 1272-1295.
[10] Chénais, S., & Forget, S. (2012). Recent advances in solid-state organic lasers. Polymer International, 61(3), 390-406.
[11] Kuehne, A. J., & Gather, M. C. (2016). Organic lasers: recent developments on materials, device geometries, and fabrication techniques. Chemical Reviews, 116(21), 12823-12864.
[12] Jiang, Y., Liu, Y. Y., Liu, X., Lin, H., Gao, K., Lai, W. Y., & Huang, W. (2020). Organic solid-state lasers: a materials view and future development. Chemical Society Reviews, 49(16), 5885-5944.
[13] Wang, Y., Han, X., Jin, L., Meng, Y., Jiang, C., Asare-Yeboah, K., ... & Bi, S. (2023). Excitation Threshold Reduction Techniques for Organic Semiconductor Lasers: A Review. Coatings, 13(10), 1815.
[14] Baldo, M. A., Holmes, R. J., & Forrest, S. R. (2002). Prospects for electrically pumped organic lasers. Physical Review B, 66(3), 035321.
[15] Lehnhardt, M., Riedl, T., Weimann, T., & Kowalsky, W. (2010). Impact of triplet absorption and triplet-singlet annihilation on the dynamics of optically pumped organic solid-state lasers. Physical Review B—Condensed Matter and Materials Physics, 81(16), 165206.
[16] Aziz, H., Popovic, Z. D., Hu, N. X., Hor, A. M., & Xu, G. (1999). Degradation mechanism of small molecule-based organic light-emitting devices. Science, 283(5409), 1900-1902.
[17] Aziz, H., & Popovic, Z. D. (2004). Degradation phenomena in small-molecule organic light-emitting devices. Chemistry of Materials, 16(23), 4522-4532.
[18] Kondakov, D. Y., Lenhart, W. C., & Nichols, W. F. (2007). Operational degradation of organic light-emitting diodes: Mechanism and identification of chemical products. Journal of Applied Physics, 101(2).
[19] Baldo, M. A., O'brien, D. F., Thompson, M. E., & Forrest, S. R. (1999). Excitonic singlet-triplet ratio in a semiconducting organic thin film. Physical Review B, 60(20), 14422.
[20] Reineke, S., & Baldo, M. A. (2014). Room temperature triplet state spectroscopy of organic semiconductors. Scientific reports, 4(1), 3797.
[21] Yoshida, K., Gong, J., Kanibolotsky, A. L., Skabara, P. J., Turnbull, G. A., & Samuel, I. D. (2023). Electrically driven organic laser using integrated OLED pumping. Nature, 621(7980), 746-752.
[22] Endo, A., Sato, K., Yoshimura, K., Kai, T., Kawada, A., Miyazaki, H., & Adachi, C. (2011). Efficient up-conversion of triplet excitons into a singlet state and its application for organic light emitting diodes. Applied Physics Letters, 98(8).
[23] Goushi, K., Yoshida, K., Sato, K., & Adachi, C. (2012). Organic light-emitting diodes employing efficient reverse intersystem crossing for triplet-to-singlet state conversion. Nature Photonics, 6(4), 253-258.
[24] Uoyama, H., Goushi, K., Shizu, K., Nomura, H., & Adachi, C. (2012). Highly efficient organic light-emitting diodes from delayed fluorescence. Nature, 492(7428), 234-238.
[25] Tao, Y., Yuan, K., Chen, T., Xu, P., Li, H., Chen, R., ... & Huang, W. (2014). Thermally activated delayed fluorescence materials towards the breakthrough of organoelectronics. Advanced materials, 26(47), 7931-7958.
[26] Wong, M. Y., & Zysman-Colman, E. (2017). Purely organic thermally activated delayed fluorescence materials for organic light-emitting diodes. Advanced Materials, 29(22), 1605444.
[27] Liu, Y., Li, C., Ren, Z., Yan, S., & Bryce, M. R. (2018). All-organic thermally activated delayed fluorescence materials for organic light-emitting diodes. Nature Reviews Materials, 3(4), 18020.
[28] Dias, F. B., Penfold, T. J., & Monkman, A. P. (2017). Photophysics of thermally activated delayed fluorescence molecules. Methods and applications in fluorescence, 5(1), 012001.
[29] Penfold, T. J., Dias, F. B., & Monkman, A. P. (2018). The theory of thermally activated delayed fluorescence for organic light emitting diodes. Chemical communications, 54(32), 3926-3935.
[30] Chen, X. K., Kim, D., & Brédas, J. L. (2018). Thermally activated delayed fluorescence (TADF) path toward efficient electroluminescence in purely organic materials: molecular level insight. Accounts of Chemical Research, 51(9), 2215-2224.
[31] Hatakeyama, T., Shiren, K., Nakajima, K., Nomura, S., Nakatsuka, S., Kinoshita, K., ... & Ikuta, T. (2016). Ultrapure Blue Thermally Activated Delayed Fluorescence Molecules: Efficient HOMO-LUMO Separation by the Multiple Resonance Effect. Advanced Materials (Deerfield Beach, Fla.), 28(14), 2777-2781.
[32] Tang, X., Cui, L. S., Li, H. C., Gillett, A. J., Auras, F., Qu, Y. K., ... & Liao, L. S. (2020). Highly efficient luminescence from space-confined charge-transfer emitters. Nature Materials, 19(12), 1332-1338.
[33] Luo, X. F., Xiao, X., & Zheng, Y. X. (2024). Recent progress in multi-resonance thermally activated delayed fluorescence emitters with an efficient reverse intersystem crossing process. Chemical Communications, 60(9), 1089-1099.
[34] Lin, S., Ou, Q., & Shuai, Z. (2022). Computational selection of thermally activated delayed fluorescence (TADF) molecules with promising electrically pumped lasing property. ACS Materials Letters, 4(3), 487-496.
[35] Li, R., & Shuai, Z. (2024). Computational screening of multi-resonance thermally activated delayed fluorescence (MR-TADF) molecules for lasing application. Organic Electronics, 132, 107095.
[36] Nakanotani, H., Furukawa, T., Hosokai, T., Hatakeyama, T., & Adachi, C. (2017). Light amplification in molecules exhibiting thermally activated delayed fluorescence. Advanced Optical Materials, 5(12), 1700051.
[37] Kim, D. H., D'aléo, A., Chen, X. K., Sandanayaka, A. D., Yao, D., Zhao, L., ... & Adachi, C. (2018). High-efficiency electroluminescence and amplified spontaneous emission from a thermally activated delayed fluorescent near-infrared emitter. Nature Photonics, 12(2), 98-104.
[38] Ye, H., Kim, D. H., Chen, X., Sandanayaka, A. S., Kim, J. U., Zaborova, E., ... & Adachi, C. (2018). Near-infrared electroluminescence and low threshold amplified spontaneous emission above 800 nm from a thermally activated delayed fluorescent emitter. Chemistry of Materials, 30(19), 6702-6710.
[39] Huang, H., Yu, Z., Zhou, D., Li, S., Fu, L., Wu, Y., ... & Fu, H. (2019). Wavelength-turnable organic microring laser arrays from thermally activated delayed fluorescent emitters. Acs Photonics, 6(12), 3208-3214.
[40] Zhou, Z., Qiao, C., Wang, K., Wang, L., Liang, J., Peng, Q., ... & Zhao, Y. S. (2020). Experimentally Observed Reverse Intersystem Crossing-Boosted Lasing. Angewandte Chemie International Edition, 59(48), 21677-21682.
[41] Khan, A., Tang, X., Zhong, C., Wang, Q., Yang, S. Y., Kong, F. C., ... & Liao, L. S. (2021). Intramolecular-locked high efficiency ultrapure violet-blue (CIE-y< 0.046) thermally activated delayed fluorescence emitters exhibiting amplified spontaneous emission. Advanced Functional Materials, 31(15), 2009488.

[42] Li, Y., Wang, K., Liao, Q., Fu, L., Gu, C., Yu, Z., & Fu, H. (2021). Tunable triplet-mediated multicolor lasing from nondoped organic TADF microcrystals. Nano Letters, 21(7), 3287-3294.
[43] Li, S., Jin, X., Yu, Z., Xiao, X., Geng, H., Liao, Q., ... & Fu, H. (2021). Design of thermally activated delayed fluorescent emitters for organic solid-state microlasers. Journal of Materials Chemistry C, 9(23), 7400-7406.
[44] Li, S., Chen, J., Wei, Y., De, J., Geng, H., Liao, Q., ... & Fu, H. (2022). An Organic Laser Based on Thermally Activated Delayed Fluorescence with Aggregation-Induced Emission and Local Excited State Characteristics. Angewandte Chemie International Edition, 61(39), e202209211.
[45] Yan, C. C., Wang, X. D., & Liao, L. S. (2022). Thermally activated delayed fluorescent gain materials: harvesting triplet excitons for lasing. Advanced Science, 9(16), 2200525.
[46] Gao, C., Miao, Z., Wong, W. W., Smith, T. A., Lo, S. C., Hu, W., ... & Dong, H. (2024). Management and utilization of triplet excitons in organic optoelectronic devices. Fundamental Research.
[47] Etherington, M. K., Gibson, J., Higginbotham, H. F., Penfold, T. J., & Monkman, A. P. (2016). Revealing the spin–vibronic coupling mechanism of thermally activated delayed fluorescence. Nature Communications, 7(1), 13680.
[48] Hestand, N. J., & Spano, F. C. (2018). Expanded theory of H-and J-molecular aggregates: the effects of vibronic coupling and intermolecular charge transfer. Chemical reviews, 118(15), 7069-7163.
[49] Mei, J., Leung, N. L., Kwok, R. T., Lam, J. W., & Tang, B. Z. (2015). Aggregation-induced emission: together we shine, united we soar!. Chemical reviews, 115(21), 11718-11940.